Supporting Information

Gilani et al. 10.1073/pnas.1316488111

SI Materials and Methods

Animals and Treatments. All experimental studies were approved by the New York State Psychiatric Institute Animal Care and Use Committee in accordance with the Guide for the Care and Use of Laboratory Animals (1) and the regulations of the National Institutes of Health Office of Laboratory Animal Welfare. The cyclin D2 (Ccnd2) knockout was produced through excision of exons I and II as described (2). Through heterozygote-heterozygote (het-het) breedings, the line was backcrossed onto a C57/BL/6 background and maintained with quarterly introduction of new C57/BL/6 wild-type breeders to the colony. Wild-type ($Ccnd2^{+/+}$) and homozygous null ($Ccnd2^{-/-}$) sex-matched siblings or colonymates obtained from het-het breedings were used for all experiments. Mice were house under standard conditions in groups of three to five.

Tissue Processing and Immunohistochemistry. Mice were perfused with PBS, followed by phosphate-buffered 4% (wt/vol) paraformaldehyde (PFA). The brains were removed and postfixed in PFA for 1 h then cryprotected by successive transfers to 10, 20, and 30% sucrose (in 0.1 M phosphate buffer) over 3 d at 4 °C. The brain was sectioned in its entirety according to the principles of systematic random sampling (3). Briefly, sectioning was initiated at a random starting point, 40-μm-thick sections were then collected serially into five equivalent sets (each with intersection thickness of 200 μm). Sets were stained as described below.

Primary antibodies included anti-mouse PV (Swant; 1:1,000), anti-rat somatostatin (Chemicon/Millipore; 1:200), anti-rabbit GABA (Sigma-Aldrich; 1:1,000), anti-rabbit or anti-chicken GFP (Molecular Probes/Invitrogen, 1:1,000), and anti-goat doublecortin (DCX), 1:500, Santa Cruz Biotechnology; SC 8,066). Staining was performed by using standard immunohistological staining protocols. Sections were washed in 0.1 M PBS and quenched in 0.3% H_2O_2 in 0.1 M PBS/CH_3OH (1:1) for 15 min at room temperature, then washed and blocked in 10% normal donkey, 0.1% bovine, or 1–2% normal goal serum in 0.1 M PBS with 0.5% Triton X-100 for 30 min^{-2}·h at room temperature. Sections were then incubated for 24–48 h at 4 °C (most primary antibodies) or slightly heated above room temperature for 24 h for DCX. Following rinsing with 0.1 M PBS, sections were incubated with a biotinylated secondary antibody. For most experiments, fluorescent secondary antibodies were used (Rhodamine Red, DyLight 488, Dylight 405, and DyLight 647; Jackson ImmunoResearch, diluted to 1:250 or 1:200). For a subset of brains stained for PV, a goat anti-mouse IgG (1:200 in PB containing 0.1% BSA and 0.25% Triton X-100) was used and revealed with a standard avidin-biotin-peroxidase reaction method (Vectastain Elite Kit; 1:100 in 0.1 M phosphate buffer; Vector Laboratories).

Quantification of Labeled Neurons. PV^+ interneuron number and density were obtained by 2D modified unbiased sampling methods (3), using a Zeiss AxioImager M2 microscope with Apotome (Carl Zeiss) integrated components for semiautomated quantitative neuroanatomy (integrated system distributed by Microbrightfield Biosciences), including an X-Y motorized stage (Ludl Electronics) and high-resolution digital video monochrome (Hamamatsu) and color (Microbrightfield Bioscience) cameras optimized for epifluorescence. These components were interfaced with a PC workstation running Stereoinvestigator software (MicroBrightfield Biosciences) for quantitative neuroanatomy. Interneurons were counted in the hippocampus (HIPP), somatosensory/motor (SS-M), and prefrontal cortices (mPFC) by using boundaries as defined by Paxinos and Franklin (4). Cells were counted in every fifth stained section (one 40-μm section per 200 μm) (*i*) throughout the rostrocaudal extent of the HIPP starting at (relative to Bregma and dural surface) anterior-posterior (AP) −1.06 mm, medio-lateral (ML) 0–1.4 mm, dorso-ventral (DV) 0.6–2.2 mm, and spanning the entire CA regions and curving posteriorly through AP −3.88 mm, ML 2.0–3.0 mm, DV −2.0 to −4.0 mm. (*ii*) The mPFC ROI spanned anteriorly from the prelimbic and medial orbital cortex, starting at AP +2.96 mm, ML 0.0–0.8 mm, DV 0.0–2.5 mm, and extending posteriorly to include entire regions of cingulate cortex, areas 1 and 2, and infralimbic cortex, and ending at the posterior limit of the later at AP +1.34 mm, ML +0.8 mm, DV −3.2 mm. Medial and lateral borders were defined by the midline and medial border of forceps minor of the corpus callosum (posteriorly). (*iii*) For the region of interest (ROI) of the SS-M, ventrolateral border was defined by a perpendicular to the pial surface at 1.0 mm dorsal to rhinal fissure and the dorsomedial boundary was set at the lateral border of the cingulate cortex 0.8–1.0 mm lateral from the midline. Cortex within these boundaries was sampled from 2.46 mm anterior to Bregma to 1.94 mm posterior to Bregma, with the ROI staying dorsal to the external capsule. For each animal, cell counts were summed across all sections. Density was calculated by dividing the total cells counted by the average ROI area as determined with the Cavalieri estimator (3) and compared between genotypes by using independent (Student's) *t* tests.

In Vitro Slice Electrophysiology. $Ccnd2^{-/-}$ and sex-matched $Ccnd2^{+/+}$ littermates, ages 3–6 wk, were anesthetized with ketamine (90 mg/kg)/xylazine (10 mg/kg) mixture. After decapitation, brains were immediately transferred to ice cold solution (220 mM sucrose, 10 mM D-glucose, 2.5 mM KCl, 26 mM $NaHCO_3$, 1.25 mM NaH_2PO_4, 2 mM $CaCl_2$, and 2 mM $MgCl_2$). Tissue block containing either the hippocampus or the PFC was mounted on a vibratome (Leica VT1200, Leica Microsystems), and 400-μm-thick horizontal (hippocampus) or coronal (PFC) slices were made. After 1 h preincubation at room temperature (24 °C) in oxygenated artificial cerebrospinal fluid containing (aCSF; 124 mM NaCl, 3 mM KCl, 26 mM $NaHCO_3$, 1.25 mM NaH_2PO_4, 1 mM $CaCl_2$, 1 mM $MgSO_4$, and 10 mM D-glucose), each slice was transferred to the recording chamber, perfused with oxygenated aCSF at 2–3 mL/min with a gravity-fed system. Pyramidal cells in the PFC or the CA1 region of hippocampus were identified with Nomarski optics on an upright fixed-stage microscope (Zeiss Axioskop FS). Whole-cell voltage-clamp recordings were performed with an Axopatch 200B amplifier (Molecular Devices). Borosilicate glass capillary pipettes (1.2 mm outer diameter) with resistance of 3–5 MΩ were filled with CsCl solution (140 mM CsCl, 2 mM $MgCl_2$, 0.1 mM $CaCl_2$, 10 mM Hepes, and 1 mM EGTA at pH 7.3 adjusted with NaOH) to record $GABA_A$ events. For measurement of glutamate events, CsCl was replaced with 140 mM K^+-gluconate. The series resistance was measured by applying voltage steps of 5 mV at the beginning and the end of each recording session and was typically between 20 and 40 MΩ. The series resistance was compensated offline to avoid adding excessive baseline noise during recording.

To isolate GABAergic miniature inhibitory postsynaptic currents (mIPSCs), tetrodotoxin (TTX; 1 μM), 2-amino-5-phosphonopentanoic acid (AP5; 50 μM), and 6-cyano-7-nitroquinoxaline-2,3-dione (CNQX; 40 μM) were added to perfusion solution. GABAA nature of mIPSC was confirmed by application of gabazine (SR95531, 20 μM) in some recordings. $GABA_A$ mIPSCs

were recorded at −70 mV. Because reversal potential of Cl^- with CsCl solution was approximately 0 mV, GABAA currents were recorded as inward. To isolate glutamatergic miniature excitatory postsynaptic currents (mEPSCs), TTX and gabazine were added to the perfusion solution, and glutamatergic nature was confirmed with application of CNQX and AP5. Glutamatergic mEPSCs were recorded at −80 mV. Liquid junction potential (~12 mV for K^+-gluconate solution) was adjusted online.

Data were filtered at 5 kHz and digitized at 10 kHz. Analysis was done in MiniAnalysis software (Synaptosoft) by using a low-pass elliptic filter (1 kHz cutoff) to remove high frequency noise. Amplitude threshold for mPSC detection was set to three times the square root of mean of noise. Events were verified by visual inspection. Averages of mIPSC frequency, amplitude, 10–90% rise time, and 10–90% decay time were calculated from at least 100 s recording for each cell, then averaged across cells for each subject. Statistical significance was tested with independent (Student's) *t* tests. Multivariate analyses including frequency, amplitude, and decay times as variables yielded results consistent with the *t* tests.

In Vivo Functional Magnetic Resonance Imaging. Design and procedures of imaging experiments were based on methods developed by Small and coworkers (5, 6). Briefly, four sets of axial T2-weighted images were acquired sequentially to generate high-resolution (86 μm × 86 μm) cerebral blood volume (CBV) maps of the rodent brain. Each set consisted of 24 images, acquired over 16 min. The contrast agent gadodiamide was injected (13 mmol/kg i.p.) after a precontrast set was acquired. CBV was mapped as changes in the transverse relaxation rate (R2) induced by the contrast agent. CBV maps were measured from steady-state T2-weighted images as CBV R2 = ln(Spre/Spost)/TE, where TE is the effective echo time, Spre is the signal before the contrast administration, and Spost is the signal after the contrast agent reaches steady state. The derived maps were normalized to the maximum four-pixel signal value of the posterior cerebral artery. Visualized anatomical landmarks were used together with standard atlases (4) to define the ROI. The hippocampal region of interest included the CA fields, subiculum, and dentate gyrus with the ventral border approximated to be the rostrodorsal border of the medial entorhinal cortex. The borders of the PFC ROI extended anteriorly and laterally from the genu of the corpus callosum to the pial surface at approximately 1.5 mm lateral to the midline; slices at and dorsal to the caudate were used. For the cerebellum, the entire structure was included. For comparisons between live- versus killed-cell MGE transplanted mice, hippocampal CBV was expressed as a ratio to cerebellar basal CBV to control for nonspecific effects of the transplants. Independent (Student's) *t* tests were used to compare each CBV measure across genotypes.

In Vivo Single-Unit Recordings of Dopamine and Hippocampal Neurons. Stereotaxic surgery and single-unit extracellular recording and neuron sampling methods were adapted from those described (7). For ventral tegmental area (VTA) dopamine (DA) neuron recordings, mice were anesthetized with chloral hydrate. Electrodes pulled from glass pipettes (tip diameter ~1 μm; impedance 4–10 MΩ) were filled with 2 M NaCl and stereotaxically lowered into the VTA. The VTA was systematically sampled by recording from four tracks spaced 0.15 mm apart with starting coordinates of 3.3 mm posterior, ±0.8 mm lateral and 3.6–4.2 mm ventral to Bregma at the dural surface. The electrode was lowered slowly through each track to detect and characterize spontaneously active neurons. The signals from individual neurons were processed as described (7). A coronal section from a representative case, showing histological evidence of several tracks at ~3.5 mm posterior to Bregma, is shown in Fig. S6*A*. DA neurons were identified by the long-duration, triphasic waveform with the "somatodendritic notch" on the positive phase and by their tonic irregular firing and intermittent bursts (Fig. S6*B*). Bursts were defined as per the criteria of Grace and Bunney (8) (see also ref. 9). The onset of bursts were marked by an interspike interval (ISI) less than 80 ms; the first spike thereafter preceded by an ISI of greater than 160 ms was considered the last spike in the burst. Within bursts on average, spike amplitudes decreased as ISI lengthened (Fig. S6*B*). DA neurons were defined as spontaneously active if spiking was detected before the electrode moving proximal to the neuron and if the firing rate of the neuron was stable for at least 2 min after discrimination. The number of spontaneously active DA neurons per track and the average firing rate and proportion of spikes fired within bursts for each DA neuron were quantified.

For hippocampal neurons, recordings were conducted in a separate cohort of mice anesthetized with urethane. Recording methods similar to those described above were used. The hippocampus was sampled with a grid of six tracks bounded by the following coordinates: 3.0–3.2 mm posterior; ±2.9–3.3 medial, and 1.5–5.0 ventral to Bregma at the dural surface. Spontaneously active neurons were detected and, following a stable recording of at least 2 min, each neuron was classified as presumptive pyramidal projection neurons or presumptive nonpyramidal neurons based on spike waveform duration and firing rate. Spike waveforms could be sorted into two distinct sets, one triphasic with spike waveform widths ≥2 ms and the other bi- or monophasic with spike waveform durations of ≤1.2 ms. Units with waveform widths of >2 ms and firing rates between 0.1 and 5 Hz and were classified as presumptive pyramidal neurons. The firing rates of neurons in the latter set ranged from 1.5 to 54 Hz; thus short (<1.2 ms) waveform units with firing rates >1.5 Hz were classified as nonpyramidal cells, presumptive interneurons. Although there is some overlap between pyramidal and nonpyramidal populations in these spike characteristics, these selection criteria reliably segregate pyramidal neurons from interneurons in hippocampus (10-12). Units with unstable or "borderline" waveform characteristics were not included to minimize misclassification. Electrode track locations were confirmed with histological methods as described for DA neuron recordings.

The number of spontaneously active DA or hippocampal pyramidal and nonpyramidal (presumed GABAergic interneurons) neurons per track, and firing rates and burst firing frequencies were compared between $Ccnd2^{-/-}$ mice and their $Ccnd2^{+/+}$ littermates by using independent *t* tests.

Behavioral Experiments. $Ccnd2^{-/-}$ mice and sex-matched $Ccnd2^{+/+}$ littermates 2.5–4 mo of age were used for behavioral testing. Mice were habituated to handling but were otherwise behaviorally naïve for each experiment except for MGE transplant mice, for which contextual fear conditioning followed a few days after locomotor response.

Contextual fear conditioning. The experimental design was adapted from methods developed by Fanselow and coworkers (13–16); context components and CS^+ and US^+ intensities were based on Saxe et al. (17). Mice were acclimated to the testing room 1 h before the training/testing session. Two transparent plastic chambers with shock grid floors placed within a white melamine sound-attenuating chamber were used as training/testing apparatus. Each chamber featured a distinctive set of visuospatial, tactile, and odor cues, which together defined the context. For the training session, mice were placed in a distinct context (training context). Conditioned stimulus (CS^+) consisting of pure tones (85 dB, 20 s duration, 4.5 kHz) were presented at 300, 470, 580, 670, and 840 s. During the last second of each tone, a 0.7-mA scrambled current was delivered through the floor grid. Animals were returned to their home cages 980 s after the start of the experiment. Twenty-four hours later, each mouse was placed in a novel context that

was constructed with visual, tactile, and olfactory cues with a high level of contrast with training context. In novel context, mice were exposed to the conditioned tone (CS^+) only (without shock) at 300, 410, 580, 670, and 830 s. Six hours after being tested in the novel context, mice were placed in the training context for 290 s. During training and testing sessions, freezing was measured by using an automated video monitoring system (Med Associates) and was inspected visually to assure that the system was identifying freezing in animals that showed no movement except for respiration. Additional parameters for measuring freezing were bout duration of 0.25 s and motion index threshold between 2 and 5. Effects of increased exposure to training context on context learning were examined by systematically varying the duration (75 and 175 s) of context exposure (called placement to shock interval) before the first presentation of the US^+. Parameters in current study differ from those of Jaholkowski et al. (18) as follows: longer duration in the training context before delivery of the first CS^+-US^+ presentation (175 vs. 120 s); greater number of CS^+-US^+ trials during training (5 vs. 3), shorter interval between training and the context retrieval test (30 vs. 48 h). These parameters interact with the integrity of the hippocampus to modulate context-dependent fear responding (13–15) and were set to achieve reliable context conditioning in the $Ccnd2^{+/+}$ mice.

An average percent time spent exhibiting the conditioned freezing response (the CR) was calculated for three types of conditioned responses: (*i*) tone-conditioned freezing, the percentage of time spent freezing during the first tone CS^+ (20 s) in novel context, (*ii*) posttone freezing, percentage of time spent freezing during the 40–100 s following CS^+ offset for CS^+ presentations 2–5 (averaged across tones), and context-conditioned freezing, the percent time freezing in the training context, excluding the first 40 s For statistical analysis, a mixed ANOVA design was used with retrieval phase as the repeated measure and genotype as the between-subjects factor. Independent (Student's) *t* tests were used for planned comparisons to test the effect of genotype on each conditioned response type.

Open field locomotor activity. Locomotor activity was measured in a 17 × 17-inch open field box with clear walls and white floor, fitted with computer-interfaced infrared motion sensing system (Med Associates). Mice were placed in open field for 30 min, after which, amphetamine (Study 1: 2 mg/kg dissolved in isotonic saline at 0.2 mg/mL; Study 2: 2, 4, or 8 mg/kg at 0.2–0.4 mg/mL) was injected i.p. and activity was measured for another 60 min. Total activity for successive 5-min bins was analyzed. Two separate cohorts were tested many months apart, and similar results were obtained. A mixed ANOVA design with genotype and drug as factors, and time (before or after injection) as the repeated measure, was used. This analysis was followed with planned Student *t* test comparisons of genotypes within drug condition separately for baseline and postinjection locomotion.

Partial lesion of the caudal hippocampus or parietal cortex. These lesions were induced as part of study to examine the impact on local guide cannula on hippocampal function. Mice were anesthetized with isoflurane anesthesia and placed mounted on a stereotaxic frame. Following aseptic preparation of the skin and skull, small burr holes were drilled through the skull. The coordinates used to target ventrocaudal CA1 in wild-type mice were (relative to Bregma and skull surface) AP −3.0, L ±3.5, DV −2.9. For the $Ccnd2^{-/-}$ mice, coordinates were modified to adjust for smaller brain size; the coordinates were AP −2.9, L ±3.3, DV −2.7. For parietal cortex cannulations, the coordinates used were AP −2.9, L ±3.5, DV −1.4 for $Ccnd2^{+/+}$ and AP −2.9, L ±3.3, DV −1.25 for $Ccnd2^{-/-}$. To induce partial lesions to cortical regions, custommade steel guide cannula were inserted (outer diameter 0.64 mm; BD Biosciences) and tissue was disrupted through movement and saline infusion through the internal cannula. The guide cannula was then left in place for 1 wk before behavioral testing. Postmortem histological analysis confirmed that this manipulation led to a consistent and lesion of the hippocampus and overlying parietal cortex or, in the control group, a lesion limited to the posterior parietal cortex.

The locomotor response to amphetamine was tested 4–10 d after recovery from surgery with the methods described above. The outcome measure used was average locomotion 10–60 min after amphetamine and was assessed with a 2 (lesion group) × 2 (genotype) ANOVA, with independent *t* tests used for planned comparisons of genotype within lesion group.

Dissection, Dissociation, and Transplantation of Progenitor Cells from the MGE. Methods of dissection, suspension, and transplantation of cells from the MGE were adapted from those described by Anderson and coworkers (19). Transgenic mice expressing green fluorescent protein (GFP), driven by chicken β-actin promoter (20) [FVB.Cg-Tg (CAG-EGFP) B5Nagy/J Stock no. 003516, maintained on a CD1 background], were obtained from Jackson Laboratories. Breeding pairs, a homozygous pan-GFP expressing (GFP^+) male and a wild-type female were placed in the mating cages at 1700 hours and separated the next morning, (designated as embryonic day 0, E0). Dams were killed on E15.5 by cervical dislocation. GFP^+ pups, identified by fluorescence under 488-nm light, were placed in Hanks' balanced salt solution (Gibco/Invitrogen). The brains were removed and embedded in 4% (wt/vol) low melting point agarose (Invitrogen) in PBS and sliced at 250-μm-thick coronal sections on a vibrating microtome (Thermo Scientific HM650V). MGE was identified visually, and slabs of tissue corresponding to the ventral two-thirds of the MGE (Fig. 4*A*) were dissociated by using fine forceps. Samples obtained from both hemispheres of two slices from two embryos were combined and considered an individual experiment for statistical purposes. Donor cells were dissociated by trituration, centrifuged at 500 × *g* for 5 min, and resuspended in 15–30 μL of NB/B27 medium (Gibco/Invitrogen). A density of 30×10^3 live cells per microliter was obtained. For killed cell control transplants, cells (obtained as described above) were killed by repeated freeze-thaw cycles (−80 °C, 1 min × 3) immediately before transplantation. Killed-cell or live-cell suspensions were injected into the brain by using a glass pipette with a 50-μm outer tip diameter connected to a nanoinjector (Drummond Scientific). The glass pipette was then connected to the injector mounted on a stereotaxic carrier. The suspended cells were transplanted bilaterally into the hippocampi of mice, aged 6–8 wk, with two injections per hemisphere (the second injection occurring 0.5 mm rostral to the first).

Mice were anesthetized with isoflurane anesthesia and placed on a stereotaxic frame. Following aseptic preparation of the skin and skull, small burr holes were drilled bilaterally through the skull. The coordinates used to target ventrocaudal CA1 in wild-type mice were (relative to Bregma and skull surface) AP −3.0 mm, L ±3.5 mm, DV −2.9 mm. For the $Ccnd2^{-/-}$ mice, coordinates were modified to adjust for smaller brain size; the coordinates were AP −2.9, L ±3.3, DV −2.7. The glass pipette was lowered slowly into the brain, taking several minutes to reach the target region, then a volume of 3.5 μL of the suspension was ejected over 5 min in 70-nL steps, for a total deposit of 2.0×10^4 cells per hemisphere.

Statistical models are described for each experiment above. For all statistical tests, results are reported as "significant" if $P < 0.05$ and as "not significant (n.s.)" if $P > 0.25$; trends are reported individually.

1. National Research Council (1996) *Guide for the Care and Use of Laboratory Animals* (National Academy Press, Washington).

2. Sicinski P, et al. (1996) Cyclin D2 is an FSH-responsive gene involved in gonadal cell proliferation and oncogenesis. *Nature* 384(6608):470–474.

3. Mouton PR (2002) *Principals and Practices of Unbiased Stereology: An Introduction for Bioscientists* (Johns Hopkins Univ Press, Baltimore).
4. Paxinos G, Franklin KBJ (2001) *The Mouse Brain in Stereotaxic Coordinates* (Academic, San Diego).
5. Moreno H, Hua F, Brown T, Small S (2006) Longitudinal mapping of mouse cerebral blood volume with MRI. *NMR Biomed* 19(5):535–543.
6. Schobel SA, et al. (2013) Imaging patients with psychosis and a mouse model establishes a spreading pattern of hippocampal dysfunction and implicates glutamate as a driver. *Neuron* 78(1):81–93.
7. Floresco SB, West AR, Ash B, Moore H, Grace AA (2003) Afferent modulation of dopamine neuron firing differentially regulates tonic and phasic dopamine transmission. *Nat Neurosci* 6(9):968–973.
8. Grace AA, Bunney BS (1984) The control of firing pattern in nigral dopamine neurons: burst firing. *J Neurosci* 4(11):2877–2890.
9. Ungless MA, Grace AA (2012) Are you or aren't you? Challenges associated with physiologically identifying dopamine neurons. *Trends Neurosci* 35(7):422–430.
10. Lapray D, et al. (2012) Behavior-dependent specialization of identified hippocampal interneurons. *Nat Neurosci* 15(9):1265–1271.
11. Somogyi P, Klausberger T (2005) Defined types of cortical interneurone structure space and spike timing in the hippocampus. *J Physiol* 562(Pt 1):9–26.
12. Henze DA, et al. (2000) Intracellular features predicted by extracellular recordings in the hippocampus in vivo. *J Neurophysiol* 84(1):390–400.
13. Blaeser F, et al. (2006) Long-term memory deficits in Pavlovian fear conditioning in Ca2+/calmodulin kinase kinase alpha-deficient mice. *Mol Cell Biol* 26(23):9105–9115.
14. Wiltgen BJ, Sanders MJ, Anagnostaras SG, Sage JR, Fanselow MS (2006) Context fear learning in the absence of the hippocampus. *J Neurosci* 26(20):5484–5491.
15. Kim JJ, Fanselow MS (1992) Modality-specific retrograde amnesia of fear. *Science* 256(5057):675–677.
16. Quinn JJ, Wied HM, Ma QD, Tinsley MR, Fanselow MS (2008) Dorsal hippocampus involvement in delay fear conditioning depends upon the strength of the tone-footshock association. *Hippocampus* 18(7):640–654.
17. Saxe MD, et al. (2006) Ablation of hippocampal neurogenesis impairs contextual fear conditioning and synaptic plasticity in the dentate gyrus. *Proc Natl Acad Sci USA* 103(46):17501–17506.
18. Jaholkowski P, et al. (2009) New hippocampal neurons are not obligatory for memory formation; cyclin D2 knockout mice with no adult brain neurogenesis show learning. *Learn Mem* 16(7):439–451.
19. De la Cruz E, et al. (2011) Interneuron progenitors attenuate the power of acute focal ictal discharges. *Neurotherapeutics* 8(4):763–773.
20. Hadjantonakis AK, Gertsenstein M, Ikawa M, Okabe M, Nagy A (1998) Generating green fluorescent mice by germline transmission of green fluorescent ES cells. *Mech Dev* 76(1-2):79–90.

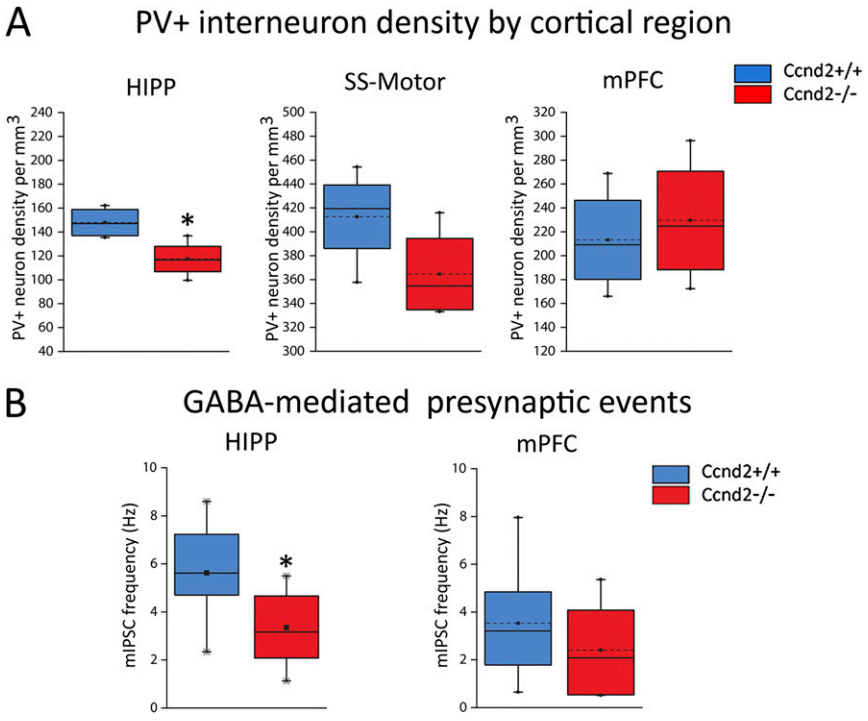

Fig. S1. Parvalbumin-expressing (PV^+) interneuron density in multiple cortical regions and corresponding data for GABA-mediated synaptic inhibition in mPFC in *Ccnd2*$^{-/-}$ and *Ccnd2*$^{+/+}$ mice. (*A*) *Ccnd2*$^{-/-}$ mice show a significant reduction in PV^+ interneuron density in the HIPP ($t_6 = 2.9$, $P < 0.05$) and a trend ($t_6 = 1.4$, $P < 0.1$) in SS-M. PV^+ interneuron density is not significantly reduced in the mPFC in the same animals. See *SI Materials and Methods* for descriptions of ROI contours. (*B*) Under conditions (and at a level of statistical power) sufficient to detect the decrease in hippocampal mIPSC frequency (Fig. 1*D*), mIPSC frequency in mPFC pyramidal cells is not significantly different in *Ccnd2*$^{-/-}$ mice ($t_{14} = 1.05$, $P > 0.25$; $n = 8$). Although the failure to find a significant decrease in PV^+ interneuron density or mIPSC frequency is not sufficient evidence to assume normal GABAergic neurotransmission in the mPFC, these results support the hypothesis that loss of CCND2 may have a relatively greater and more functional impact on PV^+ interneurons in the hippocampus than in some other cortical regions. Box plots show interquartile range, with whiskers extending to the outermost data points within 1.5x of the interquartile range. Means are marked by dotted lines running through square markers, medians by solid lines, and outliers as dots outside the whiskers. *$P < 0.05$ in independent *t* tests (one-tailed).

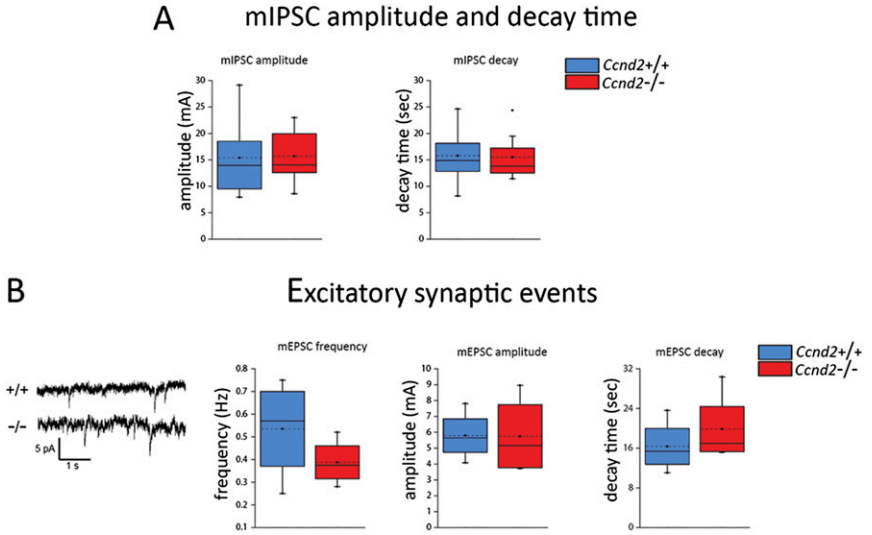

Fig. S2. Characteristics of inhibitory and excitatory synaptic currents in hippocampal CA1 pyramidal cells of *Ccnd2*$^{-/-}$ mice. (*A*) Mean amplitude and decay time of mIPSCs in CA1 pyramidal neurons do not differ significantly between *Ccnd2*$^{-/-}$ cells (red bars) and *Ccnd2*$^{+/+}$ cells (blue bars; $n = 9–10$; $P > 0.25$). (*B*) Characteristics of mEPSCs in CA 1 neurons of *Ccnd2*$^{-/-}$ and *Ccnd2*$^{+/+}$ mice. *Left* shows representative traces from whole-cell voltage clamp recordings; mEPSCs are inward (downward) current events (see *Materials and Methods* for recording conditions). Right three images show box plots of summary data for mEPSC frequency, amplitude, and decay time. There were no significant genotypic differences in these parameters of excitatory neurotransmission [$n = 6–7$, all independent *t* tests yielded nonsignificant (n.s.) results, $P > 0.25$]. Box plots show interquartile range, with whiskers extending to the outermost data points within 1.5x of the interquartile range. Means are marked by dotted lines running through square markers, medians by solid lines, and outliers as dots outside the whiskers. $*P < 0.05$, independent *t* tests (two-tailed).

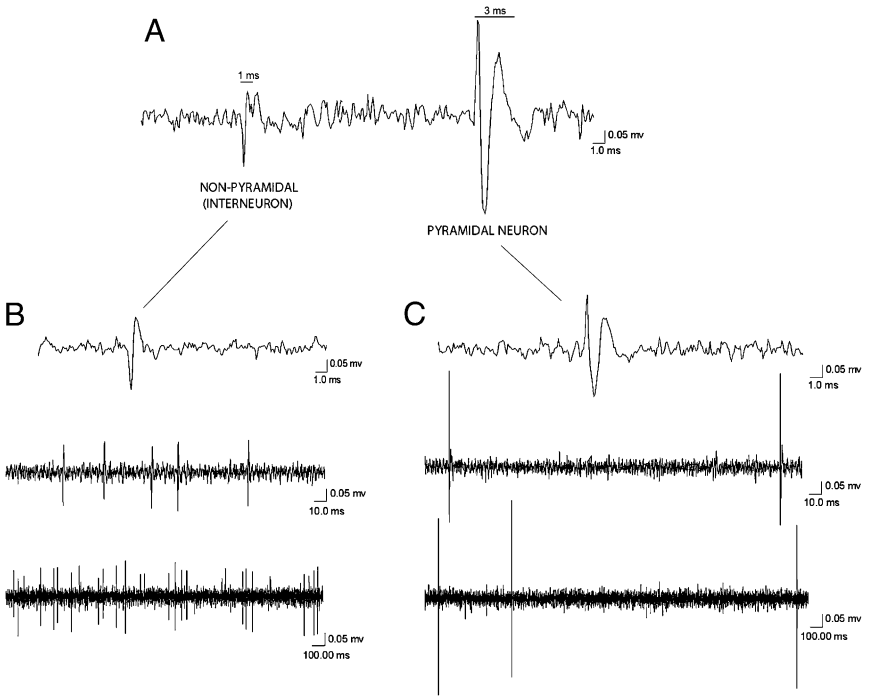

Fig. S3. Spike waveform characteristics of single units classified as pyramidal neurons or nonpyramidal (interneurons) recorded extracellularly in vivo. (*A*) Representative trace showing waveforms of two different units detected by the glass electrode. The leftmost waveform in which the duration of the spike waveform (negative and positive phases) is approximately 1 ms is typical of units classified as nonpyramidal, presumed interneurons. The triphasic, longer-duration waveform at *Right* is typical of neurons classified as pyramidal (projection) neurons. (*B*) Detail of spike waveform and spontaneous firing rate of a representative nonpyramidal unit. (*C*) Detail of spike waveform and spontaneous firing rate of a representative pyramidal unit. The firing rate criteria applied to nonpyramidal versus pyramidal units was >1.5 Hz and <5 Hz, respectively (*SI Materials and Methods*).

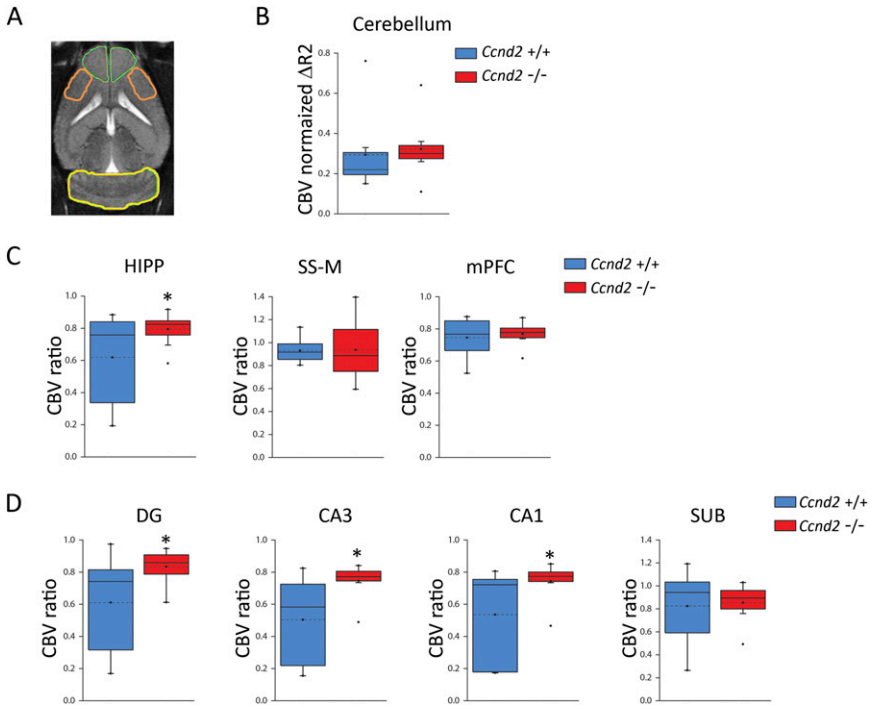

Fig. S4. Basal CBV in various cortical regions and cerebellum in *Ccnd2*$^{-/-}$ and *Ccnd2*$^{+/+}$ mice. (*A*) Structural MRI image showing ROIs for mPFC (green outline), somatosensory-motor cortex (SS-Motor) (orange outline) and cerebellum (CBL) (yellow outline) in the horizontal plane at ~2.5 mm ventral to Bregma at the skull surface. *See SI Materials and Methods* for full description of ROIs. (*B*) Basal CBV (Normalized ΔR2) for CBL in *Ccnd2*$^{-/-}$ and *Ccnd2*$^{+/+}$ mice. The difference between genotypes is not significant ($n = 7$ per genotype; $P > 0.25$). (*C*) Basal CBV in the hippocampus (HIPP), SS-Motor, and mPFC expressed as a ratio of simultaneously-measured CBV in the CBL. *Ccnd2*$^{-/-}$ mice show significantly higher CBV in the HIPP but not in SS-Motor or mPFC. (*D*) Basal CBV in hippocampal subregions. Basal CBV was significantly increased in CA1, CA3, and dentate gyrus (DG) but not in subiculum. Notably, the increase in basal CBV occurs in the context of a significant deficit in adult neurogenesis in the dentate gyrus (Fig. S7). Box plots show interquartile range, with whiskers extending to the outermost data points within 1.5x of the interquartile range. Means are marked by dotted lines running through square markers, medians by solid lines, and outliers as dots outside the whiskers. *$P < 0.05$, independent *t* tests (one-tailed).

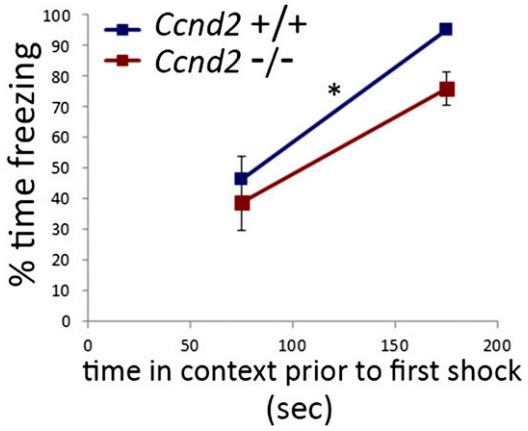

Fig. S5. Conditioned behavioral freezing in a context associated with foot shock as a function of the duration of exposure to the context before experience of the foot shock. Training consisted of exposure to five tone (CS^+)-footshock (US^+) pairings a specific context. The time between the placement of the mouse in the context and delivery of the first tone-shock pair was varied between 75 and 175 s. The conditioned response to the context was tested 30 h after training. Similar to that previously reported (14), longer exposure to the context before the first foot shock leads a stronger conditioned fear response to the context. Similar to the pattern reported for dorsal hippocampus-lesioned rodents, *Ccnd2*$^{-/-}$ mice show an overall deficit in context learning and a slight blunting of the learning slope across context exposure intervals.

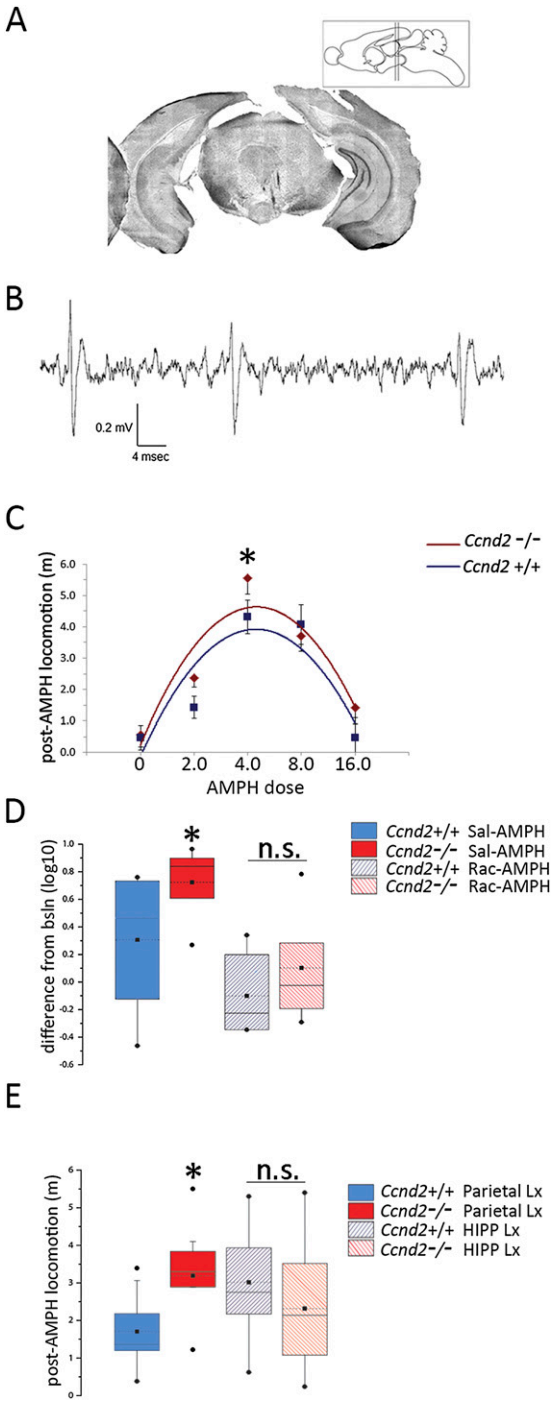

Fig. S6. Ventral tegmental area (VTA) DA neuron activity and DA-mediated locomotor phenotype in *Ccnd2*$^{-/-}$ mice. (*A*) Representative coronal section showing electrode recording tracks through the central and lateral VTA at the approximate rostro-caudal level indicated by the bar in *Inset*. (Scale bar: 1 mm, corrected for shrinkage.) (*B*) Representative trace from an extracellular recording of a single neuron. The unit exhibits waveform and burst-firing characteristics of a DA neuron (*SI Materials and Methods*). (*C*) Summary data from multiple cohorts of mice plotting average post-AMPH locomotion as a function of dose (plotted as $\log_{10}$ of dose with vehicle data shown at "0"). There is an "inverse U"-shaped dose–response function for the effect of AMPH on locomotion in both genotypes (effect of dose $F_{4,112} = 33.9$, $P < 0.001$) with *Ccnd2*$^{-/-}$ showing greater post-AMPH locomotion than *Ccnd2*$^{+/+}$ mice ($F_{1,112} = 4.9$, $P < 0.05$) [dose group mean *n*: 14.5 (veh), 24 (2.0 mg/kg), 8.5 (4.0 mg/kg), 7 (8 mg/kg), and 7.5 (16.0 mg/kg)]. (*D*) Average post-AMPH locomotion expressed as $\log_{10}$ of the mean *Ccnd2*$^{+/+}$ baseline locomotion in mice administered saline or the dopamine D2 receptor antagonist raclopride (0.5 mg/kg, i.p.) 20 min before injection of AMPH (2.0 mg/kg, i.p.). Similar to the effect shown in Fig. 3*D*, *Ccnd2*$^{-/-}$ show greater post-AMPH locomotion than *Ccnd2*$^{+/+}$ in the saline pretreatment condition. Pretreatment with raclopride blocks AMPH-induced locomotion in both genotypes, eliminating the genotypic difference. *$P < 0.05$, n.s. = $P > 0.25$ (*Ccnd2*$^{-/-}$ vs. *Ccnd2*$^{+/+}$), independent *t* tests, $n = 6$–7. (*E*) Augmented response to amphetamine in *Ccnd2*$^{-/-}$ is eliminated by partial lesions of the caudoventral hippocampus (HIPP Lx). There is a strong trend for a genotype x lesion interaction ($F_{1,30} = 3.9$, $P = 0.06$). In mice with lesion of the overlying parietal cortex, *Ccnd2*$^{-/-}$ mice show greater post-AMPH locomotion than *Ccnd2*$^{+/+}$ mice (one-tailed $t_{14} = 2.1$, $P < 0.05$; $n = 7$–9). However, following lesions of the caudoventral hippocampus, the difference between genotypes is lost (one-tailed $t_{19} = 0.77$, $P > 0.4$; $n = 10$–11). This experiment did not include nonsurgically manipulated groups, thus does not address overall differences between lesioned and nonlesioned animals. Box plots in *A* and *B* show interquartile range, with whiskers extending to the outermost data points within 1.5x of the interquartile range. Means are marked by dotted lines running through square markers, medians by solid lines, and outliers as dots outside the whiskers. *$P < 0.05$, independent *t* tests (one-tailed).

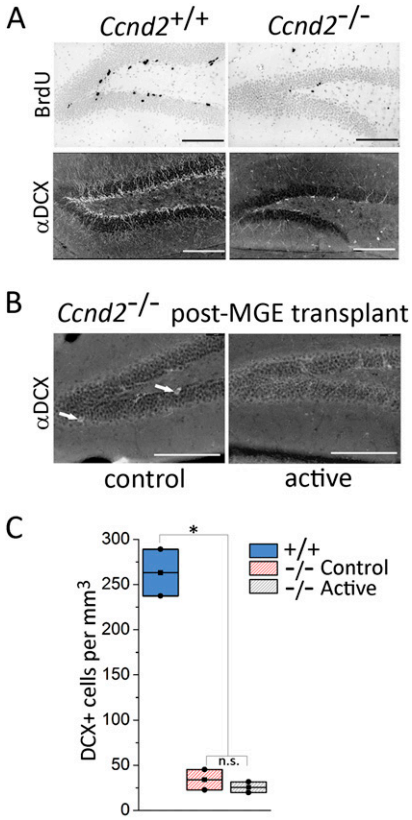

Fig. S7. The deficit in neurogenesis in the adult dentate gyrus in *Ccnd2*$^{-/-}$ mice is not ameliorated by transplantation of MGE-derived cells into the caudoventral CA fields. (*A*) Images showing mitotic cells labeled with bromodeoxyuridine (BrdU) (*Upper*; bright-field images) and neural progenitors and immature neurons labeled with DCX (*Lower*; darkfield) in wild-type (*Ccnd2*$^{+/+}$) and *Ccnd2*$^{-/-}$ adult mice. *Ccnd2*$^{-/-}$ mice show a marked reduction in neurogenesis in the adult dentate gyrus. (*B*) Neural progenitors and immature neurons labeled with DCX in the dentate gyrus of *Ccnd2*$^{-/-}$ mice 6 mo after transplantation of killed (control) or live (active) MGE-derived cells in caudoventral hippocampus. Transplants were targeted bilaterally at the caudoventral CA1. White arrows in *Left* point to DCX-labeled cells in the control transplant example. (*C*) Quantification of DCX^{+} cells in the dentate gyrus of *Ccnd2*$^{+/+}$ (sham surgery) and transplanted *Ccnd2*$^{-/-}$ adult mice. Relative to *Ccnd2*$^{+/+}$ colony mates, *Ccnd2*$^{-/-}$ mice show significantly fewer DCX^{+} neurons in the dentate gyrus. This deficit is not affected by transplantation of active MGE-derived interneuron precursors into caudoventral CA1. (Scale bars: 0.5 mm.)

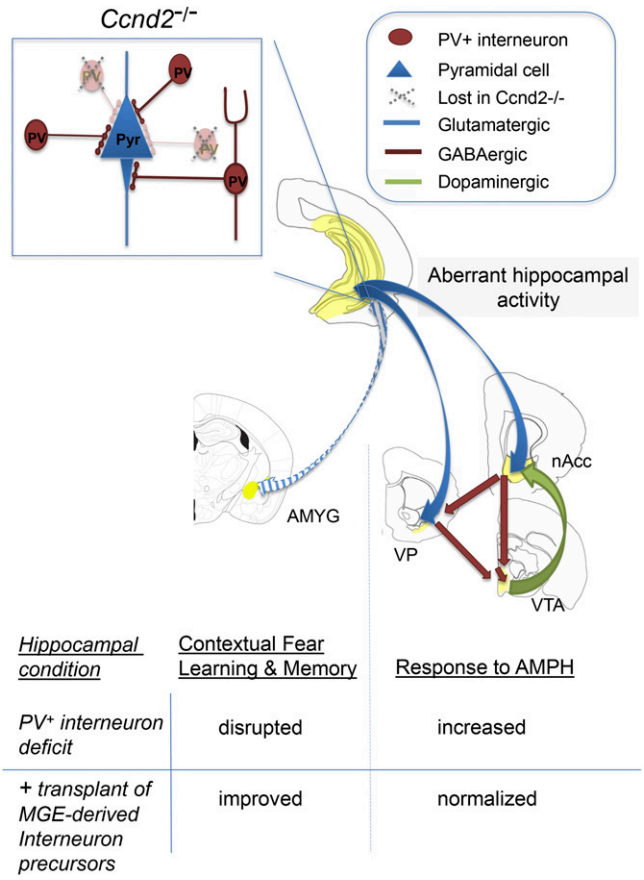

Fig. S8. The circuitry hypothesized to underlie the impact of partial PV^+ interneuron deficits on hippocampal function and the normalizing effects of MGE-derived interneuronal precursor transplants in adulthood. The blue-outlined box depicts local circuit effects of a partial loss of PV^+ interneurons, such as that produced by a knockout of *Ccnd2*. Early developmental loss of PV^+ interneurons in *Ccnd2*$^{-/-}$ mice leads to a persistent deficit in GABAergic synaptic contacts onto the perisomatic and axon hillock regions of glutamatergic projection neurons in the hippocampus. The GABA input deficit, in turn, is hypothesized to lead to disinhibition and disrupted temporal patterning (and synchronization) of signals transmitted from the ventral hippocampus to its cortical and basal forebrain targets, resulting in the disruption of cognitive operations modulated by hippocampal circuits (schematic left of blue line). The cognitive deficit observed in the present study, learning and memory of contextual information related to aversive events, is corruption of hippocampal signals to the amygdala and temporolimbic cortical regions, which, in turn, impairs learning adaptive responses to the aversive context. In parallel, the augmented signal from the hippocampus to the nucleus accumbens inhibits the activity of pallidal and tegmental GABAergic neurons that normally provide tonic inhibitory tone onto VTA DA neurons, thus disinhibiting this DA system. The increase in DA neuron activity augments ventral striatal DA-modulated behaviors including the locomotor response to AMPH. These downstream cognitive and psychomotor effects of functional deficits in hippocampal PV^+ interneurons can be mitigated in adulthood by transplanting cells harvested from the medial ganglionic eminence (MGE) at the stage of embryonic development in which the MGE is enriched with PV^+ interneuron progenitor cells.

Table S1. Qualitative assessment of sensorimotor and psychomotor behavior in Ccnd2$^{-/-}$ mice relative to Ccnd2$^{+/+}$ littermates

Ability	Test description/Ccnd2$^{+/+}$ mouse profile	Ccnd2$^{-/-}$ relative to Ccnd2$^{+/+}$ littermates
Hearing	Orients or startles to click presented within home cage	Normal
Vision	When suspended by tail and lowered toward dark (high contrast) surface, mouse reaches for surface when 20 cm above the surface.	Intact, but do not reach until <18 cm above surface
Tactile sense	Turning head toward tactile stimulus [touching hind limb with a wire (von Frey hair)].	Similar response but with increased latency
Olfaction	Obvious reaction (prolonged sniffing, digging) to new bedding; behavior	Show avoidance of new bedding
Posture	Animal is placed on all four feet, observed in standing and crouching positions, compared with Ccnd2$^{+/+}$	Normal profile
Muscle tone	Subjective rating: normal, rigid or flaccid	Normal
Ataxia/abnormal gait	Standing and ambulation without stumbling, weaving; uncoordinated ambulation; normal righting response	Normal gait; normal righting; no ataxia
Locomotor activity	Level of activity in novel environment: scale from 0–6 ranging from no movement (0) to continuous locomotion or stereotypy (6): show average score of 3 (intermittent to frequent locomotion)	Average score = 3.5 (SD = 1); may be slightly more active than *Ccnd2*$^{+/+}$ in novel environment
Response to novelty	When exposed to novel bedding or novel materials, mice explore and incorporate materials into nest	Show strong tendency to avoid novel materials